

Supplementary Materials for

Photonic-plasmonic hybrid single-molecule nanosensor measures the effect of fluorescent labels on DNA-protein dynamics

Feng Liang, Yuzheng Guo, Shaocong Hou, Qimin Quan

Published 26 May 2017, *Sci. Adv.* **3**, e1602991 (2017)

DOI: 10.1126/sciadv.1602991

This PDF file includes:

- Supplementary Text
- fig. S1. Cavity resonance measurement setup.
- fig. S2. Electrostatic calculation of nanoplasmonic enhancement.
- fig. S3. Baseline drift.
- fig. S4. Step fitting algorithm.
- fig. S5. k_{on} and k_{off} fitting.
- fig. S6. Concentration dependence of DNA-XPA interaction.
- table S1. Comparison of Q -factors and mode volumes (V).
- References (59–69)

Supplementary Text

Defining mode volumes of micro- and nanocavities

The mode volume of an optical cavity is traditionally defined in the context of enhancing spontaneous emissions, i.e. Purcell effect (59). It is defined as

$$\tilde{V}_{Purcell} = \frac{\int \epsilon |E|^2 dV}{(\epsilon |E|^2)_{\max} (\lambda/n)^3}$$

This definition, however, is not valid for dispersive and lossy systems (e.g. plasmonics). Following a framework developed by Raman et al. (60), we revisit the definition of mode volume for a system with dispersive materials. Assuming the dispersive materials are noble metals $\epsilon = \epsilon_{\infty} (1 - \frac{\omega_p^2}{\omega^2 - i\omega\gamma})$, we obtain the following set of Maxwell equation to describe the system.

$$\begin{aligned} \mu_0 \frac{\partial \mathbf{H}}{\partial t} &= -\nabla \times \mathbf{E} \\ \epsilon_{\infty} \frac{\partial \mathbf{E}}{\partial t} &= \nabla \times \mathbf{H} - \mathbf{V} \\ \frac{\partial \mathbf{P}}{\partial t} &= \mathbf{V} \\ \frac{\partial \mathbf{V}}{\partial t} &= \omega_p^2 \epsilon_{\infty} \mathbf{E} - \gamma \mathbf{V} \end{aligned}$$

\mathbf{E} and \mathbf{H} are the electromagnetic field, $\mathbf{P} = \mathbf{Ner}$ is the polarization field, \mathbf{V} is the polarization velocity field that considers free electron oscillation. Therefore, we have the eigenvalue function:

$$\omega \mathbf{A} \mathbf{x} = \mathbf{B} \mathbf{x}, \text{ and } \mathbf{x} = (\mathbf{H}, \mathbf{E}, \mathbf{V})^T$$

$$\mathbf{A} = \begin{pmatrix} \mu_0 & & \\ & \epsilon_{\infty} & \\ & & 1/(\omega_p^2 \epsilon_{\infty}) \end{pmatrix} \text{ and } \mathbf{B} = \begin{pmatrix} 0 & i\nabla \times & 0 \\ i\nabla \times & 0 & i \\ 0 & -i & i\gamma/(\omega_p^2 \epsilon_{\infty}) \end{pmatrix}$$

When $\gamma = 0$, both \mathbf{A} and \mathbf{B} are Hermitian, thus the eigenfunctions satisfy the orthogonal

condition: $\langle \mathbf{x}_m | \mathbf{A} | \mathbf{x}_n \rangle = \delta_{mn} W_n$ and $W_n = \epsilon_{\infty} |\mathbf{E}_n|^2 + \frac{\omega_p^2 \epsilon_{\infty}}{\omega^2} |\mathbf{E}_n|^2 + \mu_0 |\mathbf{H}_n|^2$.

Equivalently $W_n = \frac{d(\omega\epsilon)}{d\omega} |\mathbf{E}_n|^2 + \mu_0 |\mathbf{H}_n|^2$. Thus the classical Purcell mode volume can be generalized to

$$\tilde{V}_{Purcell} = \frac{\int W_{n=0} d\mathbf{r}}{(\epsilon |\mathbf{E}|^2)_{\max} (\lambda/n)^3}$$

In the context of single molecule sensing, we can calculate how much a single molecule changes the eigenfrequency of the system using perturbation theory. We treat single molecules as spherical nanoparticles with permittivity ϵ_m , it creates a dipole moment $p = \alpha \epsilon_\infty \mathbf{E}$ acting back to the cavity $\alpha = \frac{3(\epsilon_m - \epsilon_\infty)}{\epsilon_m + 2\epsilon_\infty} V_m \delta(r_0)$, V_m is the volume occupation of the molecule, $\delta(r_0)$ is a point function at the position of the molecule. We can also add the loss term γ into perturbation.

Therefore we have the perturbation $\mathbf{A}_I = \text{diag}(0, \alpha \epsilon_0, 0)$ and $\mathbf{B}_I = \text{diag}(0, 0, i \frac{\gamma}{\omega_p^2 \epsilon_\infty})$, we obtain

$$\Delta\omega = -\omega_{n=0} \frac{\frac{3(\epsilon_m - \epsilon_\infty)}{\epsilon_m + 2\epsilon_\infty} V_m \epsilon_0 |\mathbf{E}(r_0)|^2}{\int W_{n=0} d\mathbf{r}} + i \frac{\frac{\gamma}{\omega_p^2 \epsilon_\infty} \int |V(r_0)|^2 d\mathbf{r} |V(r_0)|^2}{\int W_{n=0} d\mathbf{r}}$$

Therefore, the resonance shift induced by the molecule as compared to the cavity full-width half-maximum (FWHM) is

$$\frac{\Delta\lambda}{\text{FWHM}} = \frac{3(\epsilon_{mol} - \epsilon_\infty)}{\epsilon_{mol} + 2\epsilon_\infty} \frac{V_{mol}}{\lambda_0^3} \frac{Q}{\tilde{V}_s} \eta.$$

λ_0 is the resonance wavelength in the vacuum, Q, \tilde{V}_s, η are dimensionless factors, defined as

$$Q = \frac{\lambda_0}{\text{FWHM}}$$

$$\tilde{V}_s = \frac{\int W_{n=0} d\mathbf{r}}{\epsilon_0 (|\mathbf{E}|^2)_{\max} (\lambda_0)^3}$$

$$\eta = \frac{|\mathbf{E}(r_0)|^2}{(|\mathbf{E}|^2)_{\max}}$$

Note that \tilde{V}_s has a slight modification from the Purcell mode volume definition $\tilde{V}_{Purcell}$ for biosensing applications. Therefore $Q\eta/\tilde{V}_s$ is a dimensionless factor, which can be compared among different micro- nanophotonic platforms, as summarized in table S1.

Electro-static calculation of plasmonic enhancement

The strong local field enhancement from nanoparticle (both resonantly and non-resonantly) can be understood by a nanoparticle-dielectric plane model, which can be solved analytically in the electro-static limit. The Maxwell equation reduces to

$$\nabla \cdot (\epsilon \mathbf{E}) = 0$$

$$\nabla \times \mathbf{E} = 0$$

E can be expressed in terms of the electrostatic potential $E = -\nabla\phi$, which satisfies Poisson's equation

$$\nabla^2\phi = 0$$

with ϕ and $\varepsilon \frac{\partial\phi}{\partial n}$ continuity at boundaries.

As is illustrated in fig. S2A, consider the case a nanoparticle of radius a and permittivity ε_m is placed in water ($\varepsilon_1=1.7$) in the upper half space $z \geq 0$. The other half plane ($z < 0$) is silicon ($\varepsilon_2=12.25$). Consider a uniform electric field E_0 is applied along the z direction. We use bi-spherical coordinates (η, ξ, φ) . The boundary is then at $\eta = 0$ (silicon plane surface) and $\eta = \eta_0$ (gold nanoparticle surface). We expand the general solution using Legendre polynomials:

$$\begin{aligned}\phi|_{\eta \geq \eta_0} &= \frac{1}{\sqrt{\cosh \eta - \cos \xi}} \sum_0^{\infty} A_n P_n(\cos \xi) e^{-(n+1/2)\eta} \\ \phi|_{\eta_0 > \eta \geq 0} &= E_0 z + \frac{1}{\sqrt{\cosh \eta - \cos \xi}} \sum_0^{\infty} P_n(\cos \xi) [B_n e^{-(n+1/2)\eta} + C_n e^{(n+1/2)\eta}] \\ \phi|_{\eta \leq 0} &= E_0 z \frac{\varepsilon_1}{\varepsilon_2} + \frac{1}{\sqrt{\cosh \eta - \cos \xi}} \sum_0^{\infty} P_n(\cos \xi) D_n e^{(n+1/2)\eta}\end{aligned}$$

The boundary condition at $\eta = 0$ leads to

$$\begin{aligned}D_n &= B_n + C_n \\ B_n &= -\Delta_2 C_n \\ \Delta_2 &= \frac{\varepsilon_2 - \varepsilon_1}{\varepsilon_2 + \varepsilon_1}\end{aligned}$$

Combined with the boundary condition at $\eta = \eta_0$, one arrives at a recursive equation

$$\alpha_n C_{n-1} - \beta_n C_n + \gamma_n C_{n+1} = \lambda_n$$

where

$$\begin{aligned}
\alpha_n &= n(e^{-\eta_0} - \Delta_1 \Delta_2 e^{-2n\eta_0}) \\
\beta_n &= (2n+1) \cosh \eta_0 - \Delta_1 \sinh \eta_0 - \Delta_1 \Delta_2 e^{-2n\eta_0} [n + (n+1)e^{-2\eta_0}] \\
\gamma_n &= (n+1)[e^{\eta_0} - \Delta_1 \Delta_2 e^{-2(n+1)\eta_0}] \\
\lambda_n &= 2^{\frac{3}{2}} E_0 d \Delta_1 [n - (n+1)e^{-2\eta_0}] e^{-2n\eta_0} \\
\Delta_1 &= \frac{\varepsilon_m - \varepsilon_1}{\varepsilon_m + \varepsilon_1} \\
\Delta_2 &= \frac{\varepsilon_2 - \varepsilon_1}{\varepsilon_2 + \varepsilon_1} \\
d &= a \sinh \eta_0
\end{aligned}$$

The recursive equation is then solved numerically with method developed by J. Love (61). The electric field can be derived as $\mathbf{E} = \frac{1}{\sqrt{\cosh \eta - \cos \xi}} \left(\frac{\partial \phi}{\partial \eta}, \frac{\partial \phi}{\partial \xi}, \frac{1}{\sin \xi} \frac{\partial \phi}{\partial \varphi} \right)$, which has a large enhancement over E_0 at small nanoparticle-plane gaps (gap size = $a \cos \eta_0 - a$). We define the enhancement factor $F = (\mathbf{E}_z / E_0)^2$.

In the antenna-in-a-nanocavity system, the nanoparticle at the central corner of the photonic crystal nanobeam cavity (Fig. 1H) decreases the mode volume of the bare photonic crystal nanobeam cavity by a factor of F , according to the volume definition. In the presence of loss, F is a complex number. Thus temperature will also be increased, which scales with $\text{Im}(F)$. Comsol multiphysics simulation is used (described in the next section) to obtain the temperature increase at a chosen frequency, at the input power level. Scaling factor $\text{Im}(F)$ is then used to obtain temperature increase across a large wavelength range. Quantum tunneling occurs at a gap size on the order of 0.5 nm (62, 63), at which point the above classical electrostatic calculations fail. In addition, the nonlocal effect will start to have significant effect on the field enhancement and mode wavelength at the gap size below 1 nm (64, 65). Considering a monolayer of 11-MUA is coated on the gold nanoparticle, we assume a ~1 nm gap between the nanoparticle and the silicon plane and apply the classical electrostatic model to our system. Advanced theoretical calculation should consider the nonlocal effect and quantum effect (66-68). As shown in fig. S2, B and C, the enhancement factor at our current operating wavelength (~1500 nm) is 20 times weaker than the maximum enhancement at the plasmon resonance (~600 nm), however, temperature increase is suppressed by more than 500. As we will show in the next section, this keeps the local temperature increase below 0.2°C in our experiment condition.

Comsol Multiphysics optical and thermal simulation

To integrate optical and heat transfer simulations, we use Comsol Multiphysics (v4.4). The Frequency Domain Electromagnetic Waves module, Eigenmode solver is used to solve the cavity resonance mode. With a single 50 nm gold nanoparticle at the central corner of the nanobeam cavity, the simulated Q -factor is 2.0×10^4 , while we measure 8.2×10^3 in experiment. Once the eigenfrequency is identified, the Frequency Domain solver is used. A waveguide mode at the resonance frequency is launched to the waveguide and the input power is set at the

experimental value. Note that the eigenfrequency from the Eigenmode solver could be slightly different from the Frequency Domain solver. After the resonance mode is identified in the Frequency Domain solver, the Heat Transfer in Fluids module can be used to solve the temperature distribution. This module solves the heat transfer equation $\rho C_p \frac{\partial T}{\partial t} - \nabla \cdot (k \nabla T) = Q_h$, where ρ is material density, C_p is the heat capacitance at constant pressure, k is the thermal conductivity and Q_h is the heat source contributed from Ohmic loss of gold nanoparticle, calculated from the Electromagnetic module. The temperature distribution at steady state is shown in Fig. 1I. At input power $5 \mu\text{W}$ at the silicon waveguide, temperature increase is about 0.2°C . Note that the simulated Q is ~ 2 times higher than the measured Q in experiment, therefore, the experimental temperature increase is even smaller ($\sim 0.1^\circ\text{C}$).

Supplementary Figures

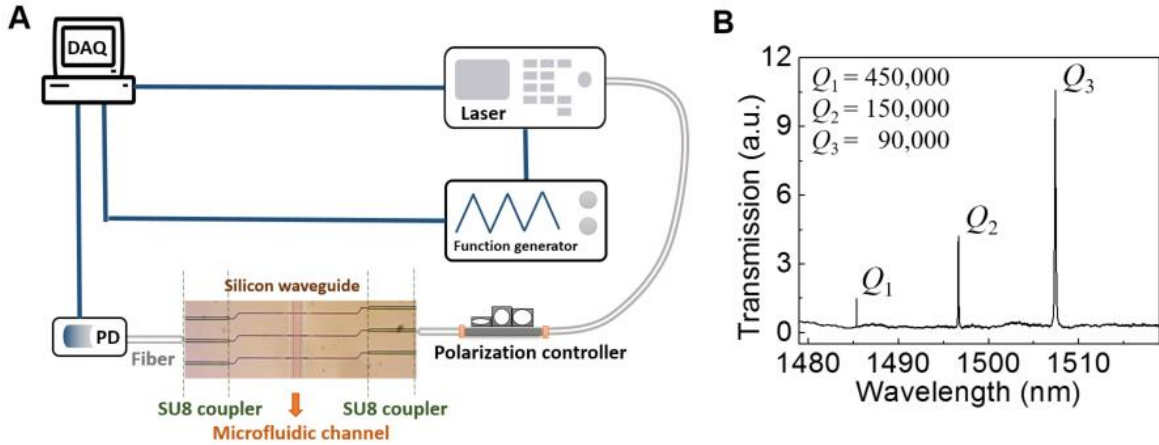


fig. S1. Cavity resonance measurement setup. (A) Schematics of the set-up. A tunable telecom laser (Santec) is scanned from 1480 nm to 1520 nm with a built-in motor. Once the resonance is detected, a function generator (HP) drives the piezo (not motor) that precisely modulates the laser frequency for a range of 100 pm around its resonance. Tapered optical fiber is used to couple light onto the chip and collect light from the chip. Polarization controller is used to filter out unwanted polarizations. The modulating signal and the collected signal from the output tapered fiber are recorded with a data acquisition system (National Instrument NI-6258). PD: photodetector. DAQ: data acquisition. (B) Typical transmission signal of a bare photonic crystal nanobeam cavity (without nanoparticle), obtained from motorized scanning, measured in air. Three cavity modes are identified in the range of 1480 nm to 1520 nm. The Q factors of the modes are obtained from Lorentzian fitting.

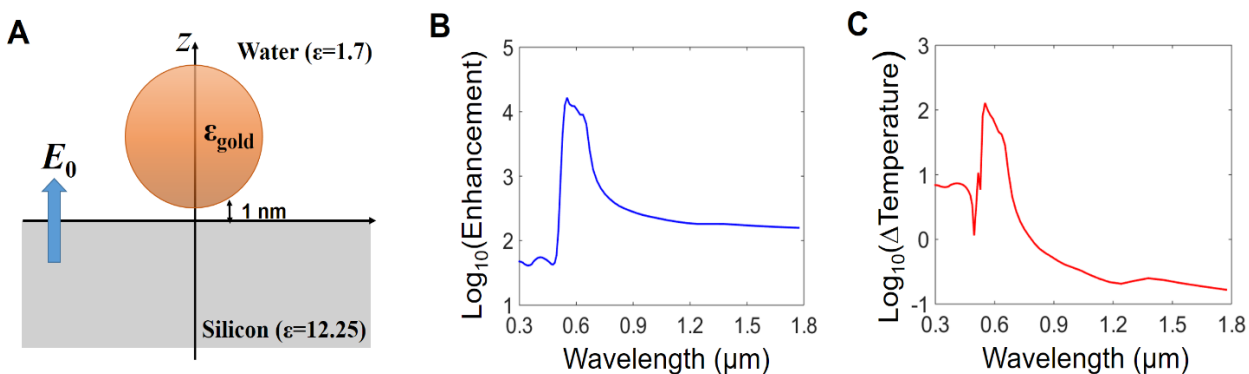


fig. S2. Electrostatic calculation of nanoplasmonic enhancement. (A) Schematics of the nanoparticle-plane model, silicon and water dielectric constants are applied for $z < 0$ and $z > 0$ half plane, respectively. A gold nanoparticle is in the $z > 0$ half plane, with 1 nm gap from the silicon-water interface ($z = 0$ plane). In our model, the nanoparticle has diameter of 50 nm and the Johnson and Christy dielectric constants of gold (69) are applied. An electromagnetic field perpendicular to the silicon-water interface is applied, which creates a large local field E_z in the gap. (B) The field intensity enhancement ($F = |E_z|/|E_0|^2$) with E_z averaged across the gap size along z direction is calculated. (C) The temperature increase due to the Ohmic loss of the gold nanoparticle.

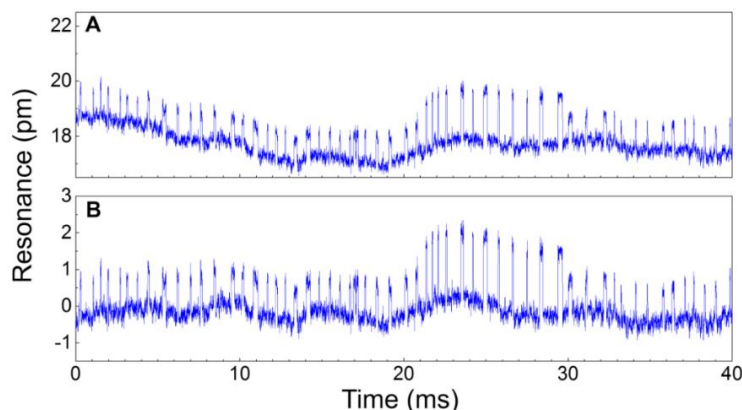


fig. S3. Baseline drift. (A) The real-time resonance trace (raw data) as a mismatched dsDNA (unlabeled) binds on and off a XPA molecule. The overall low frequency drift is from temperature fluctuations in the microfluidic channel and the mechanical drift in the set-up. (B) The slow drifts are filtered with a 9th order polynomial fitting.

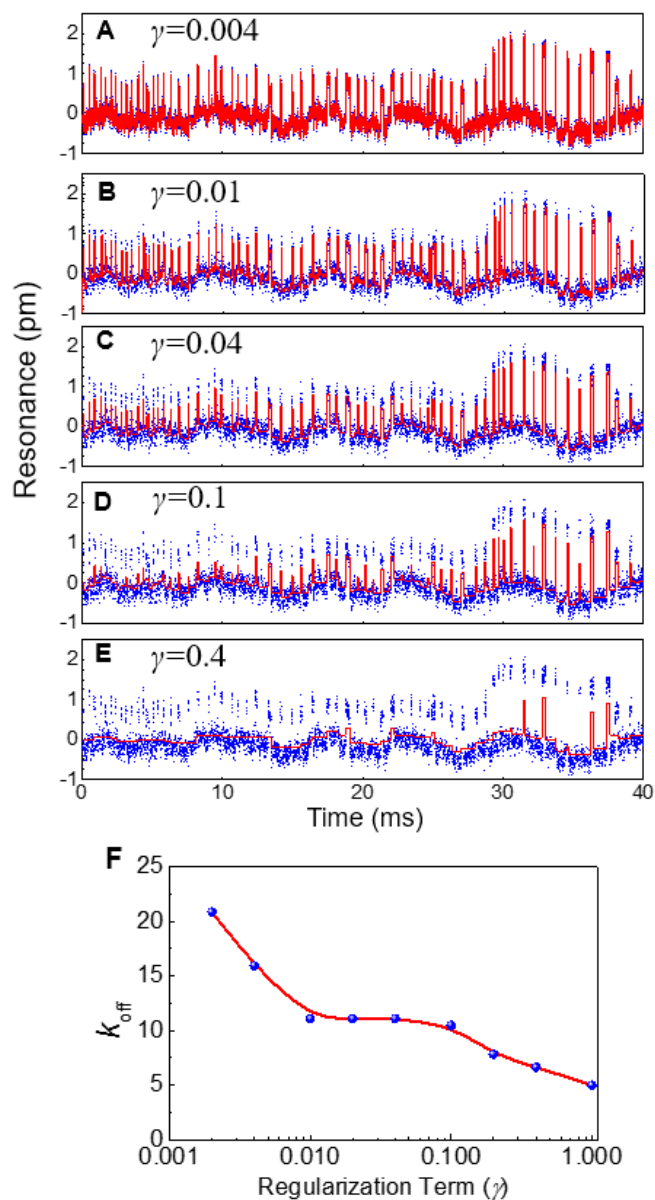


fig. S4. Step fitting algorithm. (A-E) The fitted curve (red) and original data (blue) using different regularization terms (γ). It is apparent that (A) is over-fitted and (E) is under-fitted. (F) To illustrate how to choose the value for the regularization terms (γ), k_{off} calculated using different γ s are shown. A stable region exists for k_{off} when γ values range from 0.01 to 0.1. This region gives most reliable k_{off} results, as k_{off} does not show strong dependence on γ parameter. Under these γ values, the step algorithm shows good fitting to the original data (B-D).

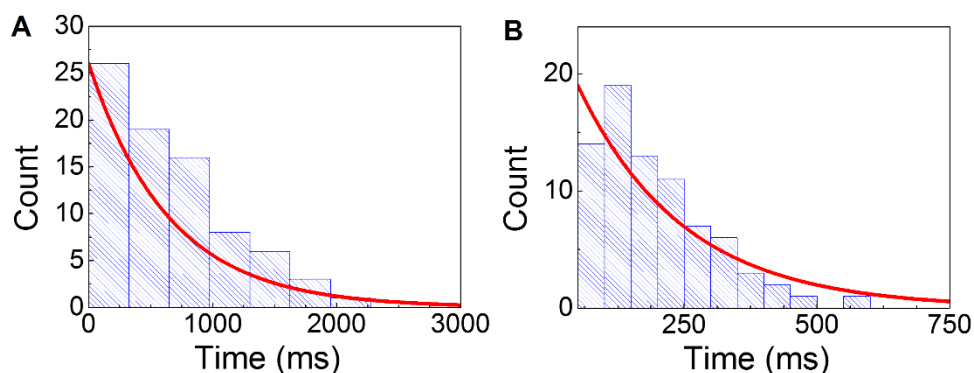


fig. S5. k_{on} and k_{off} fitting. Event histogram vs. residence time for free (unbinding) states (A) and binding states (B) for unlabeled dsDNA and XPA in the standard binding buffer. The dsDNA concentration is 10 nM. The event histogram can be fit using an exponential function: $\exp(R_{on} t)$ (red line in A) and $\exp(R_{off} t)$ (red line in B). The kinetic parameters can be derived: $k_{on} = R_{on}/\text{concentration}$, $k_{off} = R_{off}$.

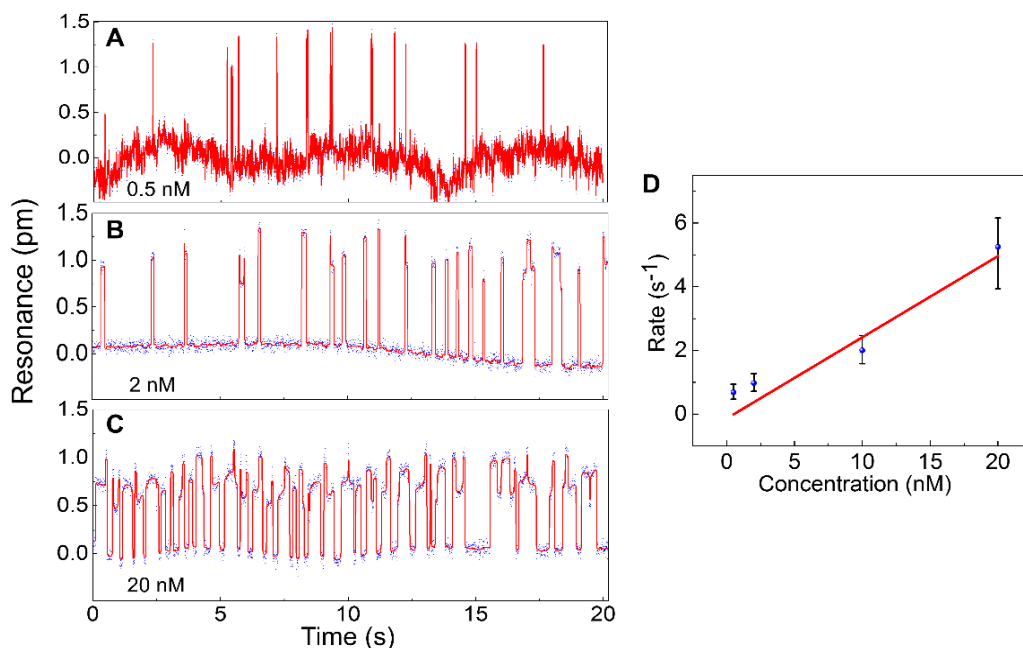


fig. S6. Concentration dependence of DNA-XPA interaction. (A-C) Real-time binding dynamics of a mismatched dsDNA (unlabeled) and XPA protein, measured at different dsDNA concentrations: 0.5 nM (A), 2 nM (B), 20 nM (C) and 10 nM (main text Fig. 3A). The frequency of the binding events increases as the concentration increases. Simultaneous multiple binding events begin to occur at concentration above 20 nM. (D) The binding event rate R is defined from the exponential fit of the event histogram at the free (unbinding) states, as shown in fig. S5. R scales linearly with the dsDNA concentration (linear fit $r^2=0.96$), indicating that single molecule events are observed at dsDNA concentration no more than 20 nM.

table S1. Comparison of Q -factors and mode volumes (V). As defined in Supplementary text, in current micro-, nano-photonic and nano-plasmonic systems. Abbreviations: WGM: whispering-gallery mode, PhC: photonic crystal cavity, SPR: surface plasmon resonance. Single molecule detection has been demonstrated in the WGM (18), SPR (20, 21), and SPR-WGM (22, 23) systems.

	Q	\tilde{V}_s	$\tilde{V}_{Purcell}$	η	$Q\eta / \tilde{V}_s$ (max)	Ref.
WGM	4×10^8 (air)	101	147	~ 0.3	1.1×10^6 (air)	(30)
2D PhC	5×10^6 (air)	0.4	1.4	~ 0.5	6.0×10^6 (air)	(31-33)
1D PhC	7.5×10^5 (air)	0.1	0.4	~ 0.6	4.5×10^6 (air)	(34)
SPR	15 (water)	1.4×10^{-5}	-	1	1.0×10^6 (water)	(20, 21, 35)
Slot-2DPhC	1.4×10^5 (air)	0.01	0.01	1	1.4×10^7 (air)	(36, 37)
	2.3×10^4 (water)	0.01	0.01		2.3×10^6 (water)	
Slot-1DPhC	1.2×10^4 (water)	0.04	0.06	1	3.0×10^5 (water)	(38)
SPR-WGM	1×10^6 (water)	1.8	-	1	5.6×10^5 (water)	(22, 23, 39)
SPR-2DPhC	720 (air)	0.2	-	1	3.6×10^3 (air)	(40, 41)
SPR-1DPhC	8.2×10^3 (water)	3.5×10^{-4}	4.6×10^{-4}	1	2.3×10^7 (water)	(current)